crystals

MDPI

Article

First Principle Study on Mg_2X (X = Si, Ge, Sn) Intermetallics by Bi Micro-Alloying

Guoning Bai, Jinzhong Tian, Qingwei Guo, Zhiqiang Li and Yuhong Zhao *

School of Materials Science and Engineering, North University of China, Taiyuan 030051, Shanxi Province, China
* Correspondence: zhaoyuhong@nuc.edu.cn

Abstract: Being a positive candidate reinforcement material for laminar composites, the Mg_2X (X = Si, Ge, Sn) based intermetallics have attracted much attention. The elastic properties, anisotropy, and electronic properties of intermetallic compounds with Bi-doped Mg_2X (X = Si, Ge, Sn) are calculated by the first principles method. Results show that the lattice parameters of Mg_2X are smaller than those of Bi-doped Mg_2X. The element Bi preferentially occupies the position of the X (X = Si, Ge, Sn) atom than other positions. Mg_2X (X = Si, Ge, Sn), $Mg_{63}X_{32}Bi$, $Mg_{64}X_{31}Bi$, $Mg_{64}Ge_{32}Bi$, and $Mg_{64}Sn_{32}Bi$ are mechanically stable, while $Mg_{64}Si_{32}Bi$ indicates that it cannot exist stably. The doping of alloying element Bi reduces the shear deformation resistance of the Mg_2X (X = Si, Ge, Sn) alloy. The pure and Bi-doped Mg_2X (X = Si, Ge, Sn) exhibits elastic and anisotropic characteristics. The contribution of the Bi orbitals of $Mg_{63}X_{32}Bi$, $Mg_{64}X_{31}Bi$, and $Mg_{63}X_{32}Bi$ are different, resulting in different hybridization effects in three types of Bi-doped Mg_2X.

Keywords: Mg_2X intermetallic compounds; first-principles; Bi micro-alloying; elastic properties; anisotropy; electronic properties

Citation: Bai, G.; Tian, J.; Guo, Q.; Li, Z.; Zhao, Y. First Principle Study on Mg_2X (X = Si, Ge, Sn) Intermetallics by Bi Micro-Alloying. *Crystals* **2021**, *11*, 142. https://doi.org/10.3390/cryst11020142

Academic Editor: Pavel Lukáč
Received: 22 December 2020
Accepted: 25 January 2021
Published: 29 January 2021

1. Introduction

Mg alloys have received extensive attention in the past decade due to their optimum strength-to-weight ratio, good corrosion resistance, high-temperature resistance, and pleasant ductility. The application of increased weight in the automotive and aerospace industries is mainly used to reduce weight and improve fuel efficiency [1–9]. The Mg_2X (X = Si, Ge, Sn) alloy has a CaF_2-type structure, which has a fairly low density and a reasonably high melting point, hardness, and modulus of elasticity [10–13]. However, Mg_2X (X = Si, Ge, Sn) alloys have severe room-temperature brittleness [14,15], resulting in a limited application range, and further research is needed.

The addition of alloying elements may improve the mechanical or electronic properties of the material [16–18]. After adding trace alloying elements, the low-temperature toughness and high-temperature creep properties of the Mg alloy can be improved by changing the lattice constant and bonding properties [16]. Experimental studies have shown that the addition of Ca in the Mg-Si alloy changes the morphology of the Mg-Si system, and improves the overall performance of the magnesium alloy; adding 0.03 wt.% Bi changes the primary Mg_2Si shape from large to irregular or dendritic to polyhedral [19,20]. Compared with other methods [21,22], the first principles method [23,24] can accurately predict the structure and properties of the phase. Using the first principles method, Zhao Hui et al. [16] showed that the doping of Ca, Sr, and Ba changed Mg_2Si from brittle to ductile; the density of the electronic states shifted, the covalent bond weakened, and the structural stability of the alloy system weakened. Rare earth elements can refine Mg-Si grains, but rare earth elements are expensive [25,26]. M. Ioannou et al. [14] found that Bi is the most stable element in Mg_2Si, compared with other dopants. Based on this, the effect of alloying element Bi on the properties of Mg_2X (X = Si, Ge, Sn) alloys was studied using the first principles method in this paper.

2. Model and Calculation Method

Mg_2X (X = Si, Ge, Sn) belongs to a cubic crystal structure. To guarantee reliable calculated results, we used a 2 × 2 × 2 supercell consisting of 96 atoms to construct the doping structures. In the supercells, Mg or X (X = Si, Ge, Sn) sites can be substituted by a single alloying element Bi, and there are many possible site preferences for Bi. In this paper, three cases were studied, respectively: (1) occupying a position of an Mg atom, (2) occupying a face center position of X (X = Si, Ge, Sn) atoms, and (3) occupying the center position between two neighboring X atoms. The calculation models are shown in Figure 1.

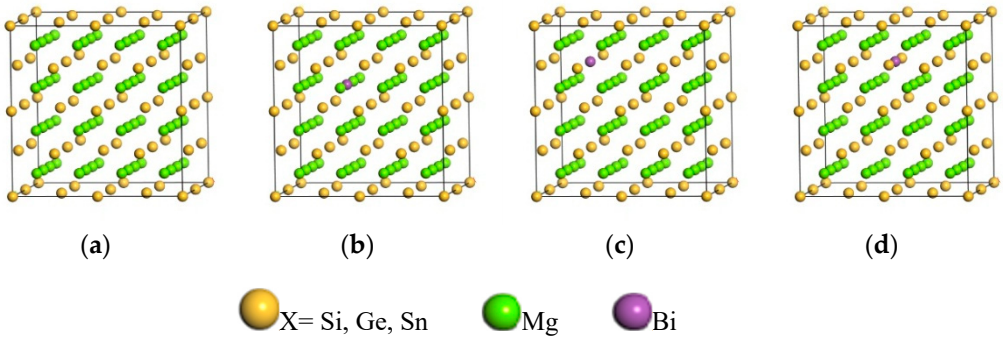

Figure 1. Cell model of (**a**) Mg_2X (X= Si, Ge, Sn), (**b**) $Mg_{63}X_{32}Bi$, (**c**) $Mg_{64}X_{31}Bi$, and (**d**) $Mg_{64}X_{32}Bi$.

The calculation process was performed using the Cambridge Serial Total Energy Package (CASTEP) [27,28], based on density functional theory (DFT) [29,30]. The electronic exchange association can adopt the GGA-PBE form [31], and the potential function selects the ultra-soft pseudopotential of the reciprocal space. The integral of the Brillouin zone was calculated by the high-symmetric *k*-point method in the form of Monkhorst-Pack [32], with the *k*-point grid being 4 × 4 × 4, and the cut-off energy for the plane wave functions was set to 380 eV for Bi-doped Mg_2X. The Broyden–Fletcher–Goldfarb–Shanno (BFGS) [33] algorithm is used to geometrically optimize the unit cell model to obtain the most stable structure. When performing self-consistent iterative SCF calculation, the Pulay density mixing method is used to solve the electron relaxation. The self-consistent convergence condition is: the total energy of the system reaches convergence within 5.0×10^{-6} eV/atom, the force on each atom is less than 0.01 eV/Å, the stress deviation is less than 0.02 GPa, the tolerance offset is less than 5×10^{-4} Å, and the SCF convergence accuracy is 5×10^{-7} eV/atom.

3. Results and Discussion

3.1. Lattice Parameters

After doping, the lattice parameters of Mg_2X (X = Si, Ge, Sn), $Mg_{63}X_{32}Bi$, $Mg_{64}X_{31}Bi$, and $Mg_{64}X_{32}Bi$ crystals are in Table 1. The predicted lattice constants of pure Mg_2X are consistent with other theoretical and experimental values [10,34–38], indicating the reliability of the present computational model. The lattice parameters of Mg_2X are smaller than those of Bi-doped Mg_2X, because the radius of doping element Bi is larger than that of alloying element X and Mg. The enthalpy of formation (ΔH_f) of Mg_2X and Bi-doped Mg_2X is shown in Equation (1):

$$\Delta H_f = \frac{E_{tot} - N_A E^A_{solid} - N_B E^B_{solid} - N_C E^C_{solid}}{N_A + N_B + N_C} \quad (1)$$

where E_{tot} represents the total energy of pure and doped Mg_2X (X = Si, Ge, Sn) phases, E^A_{soild}, E^B_{soild}, and E^C_{soild} denote the ground state energy of Mg, X, and Bi in the solid cell, N_A, N_B, and N_C are the number of Mg, X, and Bi atoms, respectively.

Table 1. Lattice constant a (Å) and enthalpy of the formation ΔH_f (eV/atom) of Mg_2X, $Mg_{63}X_{32}Bi$, $Mg_{64}X_{31}Bi$, and $Mg_{64}X_{32}Bi$ (X = Si, Ge, Sn).

Phase	Lattice Constants a/Å			ΔH_f (eV/atom)
	This Work	Cal	Exp	
pure Mg_2Si	6.371	6.30 [10]	6.35 [34]	–0.170
$Mg_{64}Si_{32}$	12.741			–0.170
$Mg_{63}Si_{32}Bi$	12.791	-	-	−0.191
$Mg_{64}Si_{31}Bi$	12.804	-	-	−0.204
$Mg_{64}Si_{32}Bi$	12.823	-	-	−0.175
pure Mg_2Ge	6.355	6.318 [35]	6.3849 [36]	−0.259
$Mg_{64}Ge_{32}$	12.710			−0.259
$Mg_{63}Ge_{32}Bi$	12.906	-	-	−0.279
$Mg_{64}Ge_{31}Bi$	12.909	-	-	−0.290
$Mg_{64}Ge_{32}Bi$	12.940	-	-	−0.264
pure Mg_2Sn	6.843	6.829 [37]	6.759 [38]	−0.196
$Mg_{64}Sn_{32}$	13.685			−0.196
$Mg_{63}Sn_{32}Bi$	13.688	-	-	−0.228
$Mg_{64}Sn_{31}Bi$	13.670	-	-	−0.237
$Mg_{64}Sn_{32}Bi$	13.711	-	-	−0.220

The calculated ΔH_f of Mg_2X and Bi-doped Mg_2X phases are listed in Table 1. The more negative ΔH_f the crystal is, the easier it is to form. The ΔH_f of $Mg_{64}X_{31}Bi$ is smaller than that of others, which indicates that the element Bi preferentially occupies the position of the X (X = Si, Ge, Sn) atom more than other positions.

3.2. Elastic Properties

The elastic constant is used to describe the ability of a material to resist external force deformation and predict the mechanical properties of a material. The elastic properties are closely related to some important thermodynamic properties (such as the Debye temperature, melting point, and specific heat capacity), so it is necessary to study the elastic properties of the alloy after Bi-doped Mg_2X (X = Si, Ge, Sn) by calculating the elastic constant.

The Bi-doped Mg_2X alloy crystals belong to the cubic crystal type, and have three independent elastic constants [39]: C_{11}, C_{12}, and C_{44}. The stability criterion is: $C_{11} - C_{12} > 0$, $C_{11} > 0$, $C_{44} > 0$, and $C_{11} + 2C_{12} > 0$ [40]. At the same time, many elastic properties of the crystal can be obtained by the elastic constant C_{ij} [41,42], for example, bulk modulus B, shear modulus G, Young's modulus E, Pugh's index of ductility B/G, Poisson's ratio ν, and anisotropic Zener ratio A_z. The calculation formula is as follows [43],

$$B = \frac{C_{11} + 2C_{12}}{3}$$

$$G_V = \frac{C_{11} - C_{12} + 3C_{44}}{5}$$

$$G_R = \frac{5(C_{11} - C_{12})C_{44}}{3(C_{11} - C_{12}) + 4C_{44}}$$

$$G = \frac{G_V + G_R}{2}$$

$$E = \frac{9BG}{3B + G}$$

$$v = \frac{3B - 2G}{2(3B + G)}$$

$$A_z = 2C_{44}/(C_{11} - C_{12})$$

In the current work, elastic constant C_{ij}, bulk modulus B, shear modulus G, Young's modulus E, Pugh's index of ductility B/G, Poisson's ratio ν, and anisotropic Zener ratio A_z of the Mg_2X, $Mg_{63}X_{32}Bi$, $Mg_{64}X_{31}Bi$, and $Mg_{64}X_{32}Bi$ alloys are shown in Table 2.

Table 2. Elastic constant C_{ij} (GPa), bulk modulus B (GPa), shear modulus G (GPa), Young's modulus E (GPa), Pugh's index of ductility B/G, Poisson's ratio ν, and anisotropic Zener ratio A_z of Mg_2X ($Mg_{64}Si_{32}$), $Mg_{63}X_{32}Bi$, $Mg_{64}X_{31}Bi$, and $Mg_{64}X_{32}Bi$ alloys.

Phase	C_{11}	C_{12}	C_{44}	B	G	E	G/B	ν	A_z
$Mg_{64}Si_{32}$	111.97	21.55	41.74	51.69	43.10	101.17	0.834	0.174	0.923z
Exp. [44]	126.00	26.00	48.50	59.00	-	-	-	-	-
Cal. [11]	121.20	23.70	49.50	56.20	49.20	113.50	-	-	-
Cal. [45]	118.80	22.27	44.96	-	-	-	-	-	-
$Mg_{63}Si_{32}Bi$	108.53	24.84	36.21	52.74	38.37	92.64	0.728	0.207	0.865
$Mg_{64}Si_{31}Bi$	107.64	24.50	36.03	52.21	38.15	92.03	0.731	0.206	0.867
$Mg_{64}Si_{32}Bi$	37.44	57.65	32.58	-	-	-	-	-	-
$Mg_{64}Ge_{32}$	103.88	19.65	37.97	49.73	39.57	93.01	0.829	0.175	0.902
Exp. [44]	117.90	23.00	46.50	54.06	-	-	-	-	-
Cal. [11]	118.10	23.60	48.00	55.10	47.70	111.10	-	0.164	-
Cal. [46]	116.10	20.60	44.00	52.50	45.40	105.9	-	0.164	-
$Mg_{63}Ge_{32}Bi$	101.58	23.26	34.24	49.37	36.13	87.14	0.732	0.206	0.874
$Mg_{64}Ge_{31}Bi$	101.25	22.21	33.86	48.56	36.02	86.64	0.742	0.203	0.857
$Mg_{64}Ge_{32}Bi$	52.54	43.72	28.52	46.66	13.91	37.96	0.298	0.364	6.472
$Mg_{64}Sn_{32}$	68.36	29.39	34.20	40.38	28.11	68.46	0.696	0.217	1.630
Exp. [47]	82.40	20.80	36.60	-	-	-	-	-	-
Cal. [11]	83.71	39.79	21.69	42.36	21.79	74.78	0.51	0.206	-
Cal. [44]	81.10	20.16	34.85	43.73	31.70	-	-	-	-
$Mg_{63}Sn_{32}Bi$	66.42	27.11	27.42	40.21	24.00	60.04	0.597	0.251	1.395
$Mg_{64}Sn_{31}Bi$	67.51	25.96	28.63	39.81	25.18	62.38	0.632	0.239	1.378
$Mg_{64}Sn_{32}Bi$	58.06	29.27	23.25	38.97	19.18	49.41	0.493	0.288	1.615

It can be found in Table 2 that Mg_2X (X = Si, Ge, Sn), $Mg_{63}X_{32}Bi$ [48], $Mg_{64}X_{31}Bi$, $Mg_{64}Ge_{32}Bi$, and $Mg_{64}Sn_{32}Bi$ satisfy the stability criterion, indicating that these crystals are mechanically stable, while $C_{11} - C_{12} < 0$ of $Mg_{64}Si_{32}Bi$ indicates that the cubic structure cannot exist stably. Thus, it is not an optimal structure.

The bulk modulus B represents the ability of materials to resist deformation under external stress, and the greater the bulk modulus, the stronger the ability to resist deformation [49]. After Bi doping Mg_2Ge and Mg_2Sn: $Mg_2X > Mg_{63}X_{32}Bi > Mg_{64}X_{31}Bi > Mg_{64}X_{32}Bi$ (X = Ge and Sn), but after Bi-doped Mg_2Si, $Mg_{63}Si_{32}Bi > Mg_{64}Si_{31}Bi > Mg_2Si$, indicating that the ability of Mg_2Si to resist deformation after doping is enhanced. The value of B for $Mg_{63}Si_{32}Bi$ is larger than that for other Bi-doped Mg_2X (X = Si, Ge, Sn) phases, indicating that the $Mg_{63}Si_{32}Bi$ has stronger deformation resistance.

The shear modulus G is used to evaluate the ability of the object to resist shear strain; the greater the value is, and the more obvious the directional bonds between the compounds are, the better the resistance to plastic deformation [50]. The doping of alloying element Bi reduces the shear deformation resistance of the Mg_2X (X = Si, Ge, Sn) alloy. The order of the deformation resistance of $Mg_{63}X_{32}Bi$, $Mg_{64}X_{31}Bi$, and $Mg_{64}X_{32}Bi$ is $Mg_{63}Si_{32}Bi > Mg_{63}Ge_{32}Bi > Mg_{63}Sn_{32}Bi$, $Mg_{64}Si_{31}Bi > Mg_{64}Ge_{31}Bi > Mg_{64}Sn_{31}Bi$, $Mg_{64}Sn_{32}Bi > Mg_{64}Ge_{32}Bi$, respectively. This means that the alloy obtained by Bi doping Mg_2Si has better shear resistance than $Mg_{63}X_{32}Bi$ and $Mg_{64}X_{31}Bi$ (X = Ge, Sn).

Young's modulus E is an important parameter to characterize material stiffness. The smaller the value, the smaller the stiffness, and the better the plasticity of the materials [49]. The doping of the alloying element Bi in Table 2 enhances the plasticity and reduces the stiffness of the Mg_2X (X = Si, Ge, Sn) alloy. The stiffness of $Mg_{63}Si_{32}Bi$ ($Mg_{64}Si_{31}Bi$) is stronger than that of other $Mg_{63}X_{32}Bi$ ($Mg_{64}X_{31}Bi$). Poisson's ratio ν refers to the ratio of the absolute value of the transverse positive strain and the axial positive strain when the material is under tension or compression in a single direction. The greater the value, the

better the plasticity the corresponding material will have [51]. It can be seen from Table 2 that the doping of the alloying element Bi enhances the plasticity of the Mg_2X (X = Si, Ge, Sn) alloy and corresponds to Young's modulus calculation result.

According to Pugh, *G/B* can predict the ductility or brittleness of materials, and the corresponding critical value is 0.57. When $G/B > 0.57$, materials are brittle, and ductile materials are opposite [52]. The doping of the alloying element Bi causes the Mg_2X (X = Si, Ge, Sn) alloy to be converted from a brittle material to a ductile material, as can be seen in Table 2. In general, the brittleness (extension) of a material can also be measured by $C_{12}-C_{44}$. If $C_{12}-C_{44} > 0$, the material exhibits ductility; on the contrary, it is brittle [16,53]. According to Table 2, it is known that the Mg_2X, $Mg_{63}X_{32}Bi$, and $Mg_{64}X_{31}Bi$ (X = Si, Ge, Sn) alloys are brittle materials, and $Mg_{64}X_{32}Bi$ (X = Ge, Sn) is a ductile material, which is consistent with the results obtained by *G/B*.

The elastic anisotropy of the material in the engineering materials shows the possibility of micro-crack in the material, which is closely related to the nanoscale precursor texture of the material, and occupies an important position in the material science [54,55]. Anisotropy, on the other hand, reflects the density distribution of electrons in different directions based on DFT calculations. In different crystal orientations, the density function of electrons is not the same, so it will show a different degree of anisotropy. The material behaves as isotropic when $A_z = 1$. According to Table 2, it can be seen that the A_z of pure and Bi-doped Mg_2X is not equal to 1, showing the anisotropy of pure and doped Mg_2X. The A_z of Mg_2Si is very close to 1, indicating that the elastic anisotropy of Mg_2Si is relatively small. The anisotropy of Bi-doped Mg_2X (X = Si, Ge) phase is larger than that of Mg_2X, whereas the anisotropy of Bi-doped Mg_2Sn is smaller than that of Mg_2Sn.

Figure 2 plots the 3D Young's modulus *E*-surface diagram of pure and Bi-doped Mg_2X (X = Si, Ge, Sn) alloys at 0 GPa. It is clear from the three-dimensional surface that the pure and Bi-doped Mg_2X phases show elastic anisotropy, because their 3D shapes deviate from the spherical shape. $Mg_{64}Ge_{32}Bi$ deviates most from the spherical shape among these phases, indicating that $Mg_{64}Ge_{32}Bi$ shows strong anisotropy. The main effect of impurity doping is mainly to change the charge density distribution, thus affecting the anisotropy. This result is consistent with the calculation results.

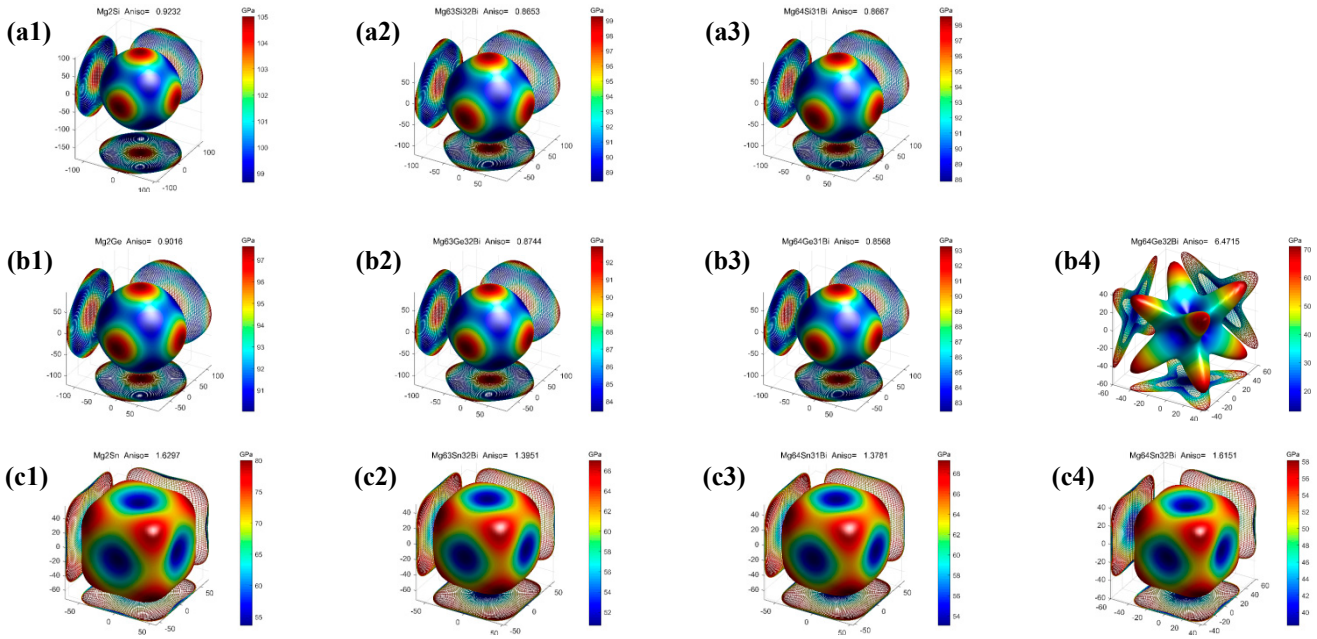

Figure 2. 3D Young's modulus *E*-surface diagram under 0 GPa, where (**1**), (**2**), (**3**) and (**4**) corresponds to different bi atom doping methods of Mg_2X (X = Si (**a**), Ge (**b**), Sn (**c**)).

3.3. Electronic Properties

Before calculating the electronic structure, we tested the influence of the spin polarization settings on the total energy of the $Mg_{63}Si_{32}Bi$ system, and the results are shown in Table 3. It can be found that the difference between total energy is very small, which means that the effect of spin polarization on the total energy and electronic structure is negligible.

Table 3. Total energy of $Mg_{63}Si_{32}Bi$ under different spin polarization settings.

	Non-Spin Polarized	Spin Polarized
Total Energy (eV)	−64958.92186	−64958.92179

Usually, we study the band gap based on the band structure. We calculated the energy band of Mg_2Si and Mg_2Ge, and the results are shown in Figure 3. It can be seen that there is a band gap of 0.223 eV in Mg_2Si and 0.123 eV in Mg_2Ge, which means that Mg_2Si and Mg_2Ge are both semiconductor materials. However, this cannot be reflected from the DOS diagram. The calculations of Mg2Si in the literature [56–58] also has similar results.

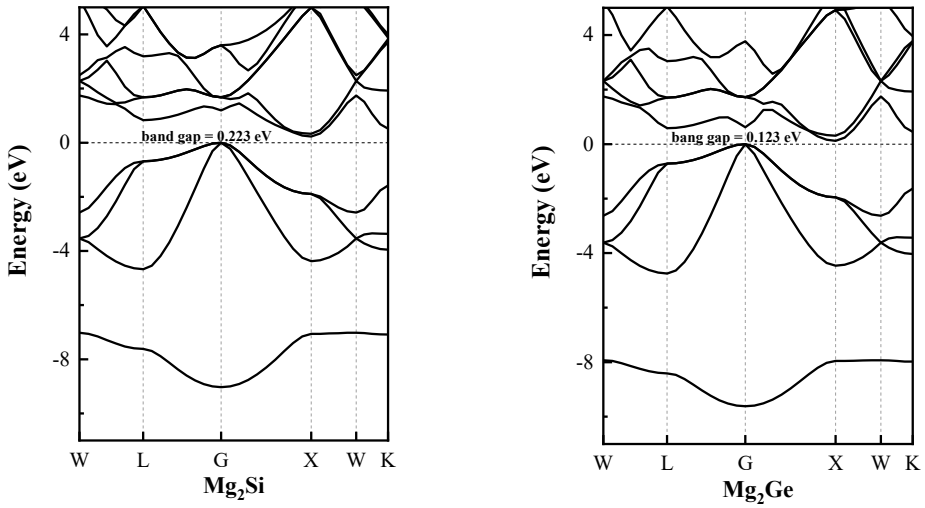

Figure 3. The band structures of Mg_2Si and Mg_2Ge.

As shown in Figure 4, the bonding electrons of the pure and Bi-doped Mg_2X (X = Si, Ge, Sn) alloy compounds are mainly distributed at −10 to 5 eVs. In an energy range from −10 to 0 eV, there is no significant difference in the shape of the total density of states (TDOS) between pure and doped Mg_2X phases. In Figure 4a, the bonding electrons mainly come from the contributions of Mg-3s, Si-3s, Ge-4s, and Sn-5s orbitals. In the −5~0 eV interval, Si-3p, Ge-4p, and Sn-5p orbitals have strong orbital hybridization with Mg-2p and Mg-3s. The energy range from 0~eV to 5~eV is mainly contributed by Mg-2p and Mg-3s orbitals, with small involvement of X states.

As shown in Figure 4b, in the energy range from −10 to −6 eV, the atomic orbital of $Mg_{63}X_{32}Bi$ (X = Si and Sn) alloys are mainly dominated by Bi-6p, Si-3s, Sn-5s, and Mg-3s states, and the TDOS of $Mg_{63}Ge_{32}Bi$ is mainly contributed by Bi-6s, Ge-4s, and Mg-3s states. In the range of −6~0 eV, the $Mg_{63}X_{32}Bi$ (X = Si, Ge, Sn) alloy mainly comes from the interaction between Mg-2p, Mg-3s, Si-3p, Ge-4p, Sn-5p, and Bi-6p, indicating that Mg, X, and Bi have strong bond binding effects in this interval. The Mg-2p and Mg-3s orbitals contribute strongly in the range of 0~5 eV for $Mg_{63}X_{32}Bi$ (X = Si, Ge, Sn).

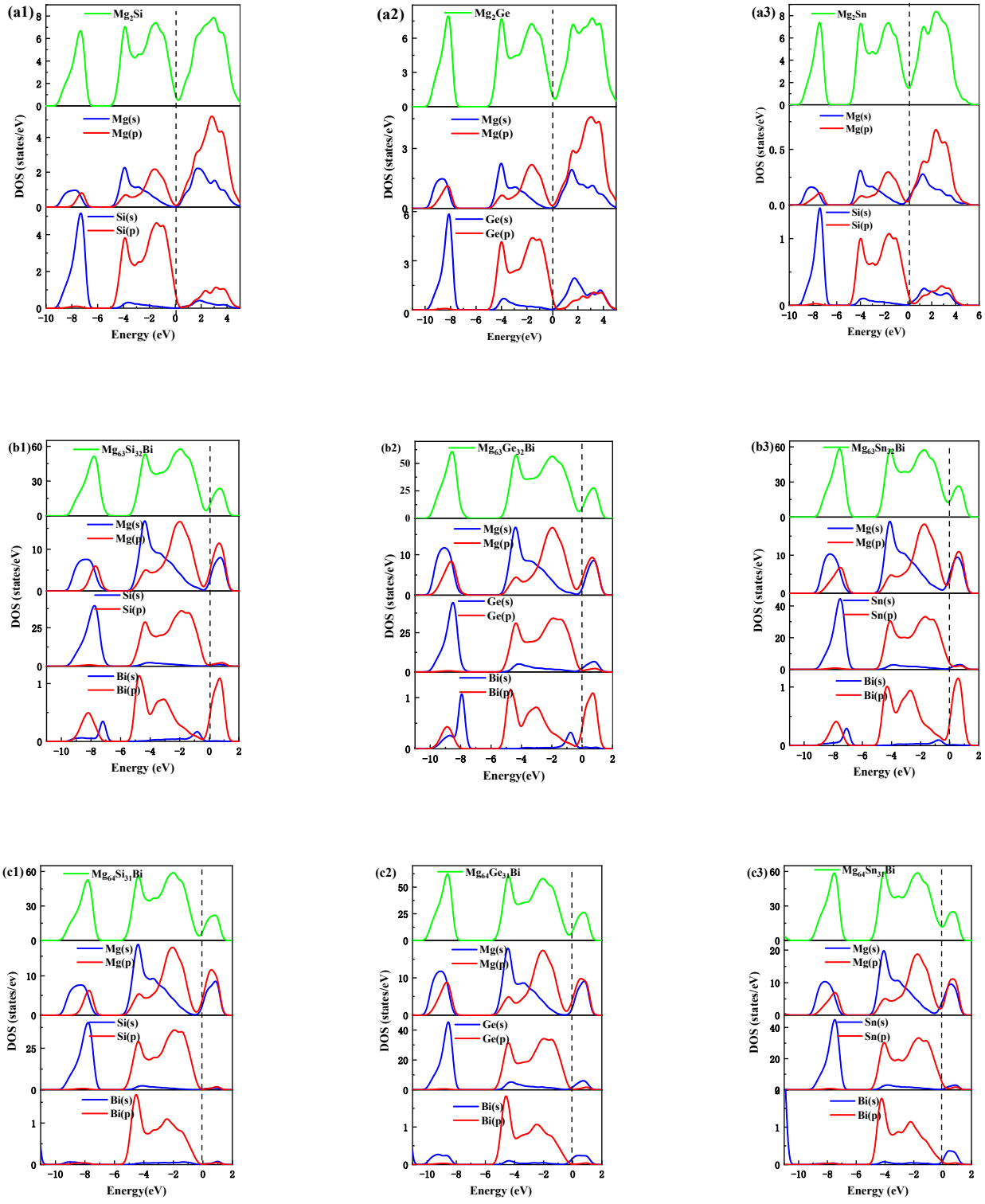

Figure 4. *Cont.*

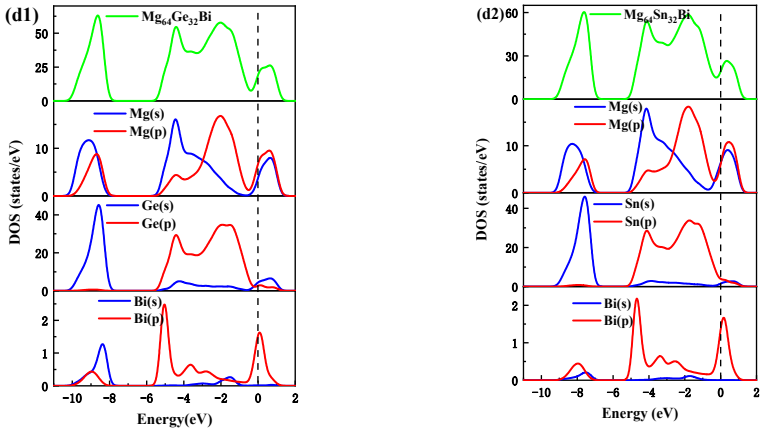

Figure 4. Total density of states and partial density of states, where (**a**–**d**) corresponds to pure and Bi-doped Mg_2X (X = Si (**1**), Ge (**2**), Sn (**3**)).

In Figure 4c, between −6 and 0 eV, the orbital contribution of the $Mg_{64}X_{31}Bi$ alloy is the same as that of the $Mg_{63}X_{32}Bi$ alloy. In the range of −10~−6 eV and 0~2 eV, the contribution of Bi-6s and Bi-6p orbitals of $Mg_{64}X_{31}Bi$ to TDOS has changed compared to $Mg_{63}X_{32}Bi$. As shown in Figure 4d, the contribution of the Mg and X (S = Ge, Sn) orbitals of $Mg_{64}X_{32}Bi$ to TDOS are similar to the analysis of $Mg_{63}X_{32}Bi$ and $Mg_{64}X_{31}Bi$. However, the contribution of Bi orbitals of $Mg_{63}X_{32}Bi$, $Mg_{64}X_{31}Bi$, and $Mg_{63}X_{32}Bi$ are different, resulting in different hybridization effects in three types of Bi-doped Mg_2X.

4. Conclusions

In this paper, the elastic properties and electronic structures of pure and Bi-doped Mg_2X (X = Si, Ge, Sn) compounds were calculated by the method of plane wave pseudopotential based on density functional theory. The calculation results show that:

(1) The lattice parameters of Mg_2X are smaller than those of Bi-doped Mg_2X, because the radius of doping element Bi is larger than that of alloying element X and Mg. The ΔH_f of $Mg_{64}X_{31}Bi$ is smaller than that of others, which indicates that the element Bi preferentially occupies the position of the X (X = Si, Ge, Sn) atom than other positions.

(2) Mg_2X (X = Si, Ge, Sn), $Mg_{63}X_{32}Bi$, $Mg_{64}X_{31}Bi$, $Mg_{64}Ge_{32}Bi$, and $Mg_{64}Sn_{32}Bi$ are mechanically stable, while $Mg_{64}Si_{32}Bi$ indicates that it cannot exist stably. The ability of Mg_2Si to resist deformation after doping is enhanced, and $Mg_{63}Si_{32}Bi$ has stronger deformation resistance. The doping of alloy element Bi makes the Mg_2X (X = Si, Ge, Sn) alloy convert from brittle material to ductile material, and results in plasticity enhancement and stiffness reduction.

(3) The pure and Bi-doped Mg_2X (X = Si, Ge, Sn) exhibit elastic anisotropic properties. The anisotropy of Bi-doped the Mg_2X (X = Si, Ge) phase is larger than that of Mg_2X, whereas the anisotropy of Bi-doped Mg_2Sn is smaller than that of Mg_2Sn. $Mg_{64}Ge_{32}Bi$ shows strong anisotropy among these phases.

(4) In an energy range from −10 to 0 eV, there is no significant difference in the shape of TDOS between the pure and doped Mg_2X phases. The contribution of Bi orbitals of $Mg_{63}X_{32}Bi$, $Mg_{64}X_{31}Bi$, and $Mg_{63}X_{32}Bi$ are different, resulting in different hybridization effects in three types of Bi-doped Mg_2X.

Author Contributions: G.B., Q.G., Z.L. performed the theoretical calculations; J.T., Y.Z. analyzed the data; G.B. wrote the paper. All authors have read and agreed to the published version of the manuscript.

Funding: This research was funded by the Science and Technology Major Project of Shanxi Province (Nos. 20181101014, 20191102008, 20191102007); National Natural Science Foundation of China (Nos. 52074246, 22008224, 51774254, 51774253, 51804279, 51801189).

Institutional Review Board Statement: The study did not require ethical approval.

Informed Consent Statement: Not applicable.

Data Availability Statement: Data is contained within the article.

Conflicts of Interest: The authors declare no conflict of interest.

References

1. Potzies, C.; Kainer, K. Fatigue of Magnesium Alloys. *Adv. Eng. Mater.* **2004**, *6*, 281–289. [CrossRef]
2. Schumann, S.; Friedrich, H.E. Current and Future Use of Magnesium in the Automobile Industry. *Mater. Sci. Forum* **2003**, *419*, 51–56. [CrossRef]
3. Kulekci, M.K. Magnesium and its alloys applications in automotive industry. *Int. J. Adv. Manuf. Technol.* **2008**, *39*, 851–865. [CrossRef]
4. Brungs, D. Light weight design with light metal castings. *Mater. Des.* **1997**, *18*, 285–291. [CrossRef]
5. Gao, X.; Nie, J. Characterization of strengthening precipitate phases in a Mg-Zn alloy. *Scr. Mater.* **2007**, *56*, 645–648. [CrossRef]
6. Friedrich, H.; Schumann, S. Research for a "new age of magnesium" in the automotive industry. *J. Mater. Process. Technol.* **2001**, *117*, 276–281. [CrossRef]
7. Chen, L.; Zhao, Y.; Hou, H.; Zhang, T.; Liang, J.; Li, M.; Li, J. Development of AZ91D magnesium alloy-graphene nanoplatelets composites using thixomolding process. *J. Alloy. Compd.* **2019**, *778*, 359–374. [CrossRef]
8. Zhang, T.; Zhao, Y.; Chen, L.; Liang, J.; Li, M.; Hou, H. Graphene Nanoplatelets Reinforced Magnesium Matrix Composites Fabricated by Thixomolding. *Acta Metall. Sin.* **2019**, *55*, 638–646. [CrossRef]
9. Cheng, P.; Zhao, Y.; Lu, R.; Hou, H. Effect of the morphology of long-period stacking ordered phase on mechanical properties and corrosion behavior of cast Mg-Zn-Y-Ti alloy. *J. Alloy. Compd.* **2018**, *764*, 226–238. [CrossRef]
10. Li, G.H.; Gill, H.S.; Varin, R.A. Magnesium silicide intermetallic alloys. *Met. Mater. Trans. A* **1993**, *24*, 2383–2391. [CrossRef]
11. Zhou, D.; Liu, J.; Xu, S.; Peng, P. Thermal stability and elastic properties of Mg_2X (X = Si, Ge, Sn, Pb) phases from first-principle calculations. *Comput. Mater. Sci.* **2012**, *51*, 409–414. [CrossRef]
12. Martin, J. Thermal conductivity of Mg_2Si, Mg_2Ge and Mg_2Sn. *J. Phys. Chem. Solids* **1972**, *33*, 1139–1148. [CrossRef]
13. Jund, P.; Viennois, R.; Colinet, C.; Hug, G.; Fèvre, M.; Tédenac, J.-C. Lattice stability and formation energies of intrinsic defects in Mg_2Si and Mg_2Ge via first principles simulations. *J. Physics Condens. Matter* **2012**, *25*, 035403. [CrossRef] [PubMed]
14. Ioannou, M.; Polymeris, G.; Hatzikraniotis, E.; Paraskevopoulos, K.; Kyratsi, T. Effect of Bi-doping and Mg-excess on the thermoelectric properties of Mg_2Si materials. *J. Phys. Chem. Solids* **2014**, *75*, 984–991. [CrossRef]
15. Li, W.X. *Magnesium and Magnesium Alloys*; Central South University Press: Changsha, China, 2005; p. 102.
16. Zhao, Y.H.; Zhao, X.M.; Yang, H.M.; Sui, H.; Hou, P.D. First-Principles Study on Elastic Properties and Electronic Structure of Ca, Sr and Ba Doped Mg_2Si. *Rare Metal. Mat. Eng.* **2015**, *44*, 638–643.
17. Wang, C.; Fu, H.; Jiang, L.; Xue, D.; Xie, J. A property-oriented design strategy for high performance copper alloys via machine learning. *npj Comput. Mater.* **2019**, *5*, 87. [CrossRef]
18. Zhao, Y.; Tian, J.; Bai, G.; Zhang, L.; Hou, H. First Principles Study on the Thermodynamic and Elastic Mechanical Stability of Mg_2X (X = Si,Ge) Intermetallics with (anti) Vacancy Point Defects. *Crystals* **2020**, *10*, 234. [CrossRef]
19. Lisitsyn, V.; Ben-Hamu, G.; Eliezer, D.; Shin, K. The role of Ca microalloying on the microstructure and corrosion behavior of Mg-6Zn-Mn-(0.5-2)Si alloys. *Corros. Sci.* **2009**, *51*, 776–784. [CrossRef]
20. Akrami, A.; Emamy, M.; Mousavian, H. The effect of Bi addition on the microstructure and tensile properties of cast Al-15%Mg_2Si composite. *Mater. Werkst.* **2013**, *44*, 431–435. [CrossRef]
21. Zhao, Y.; Zhang, B.; Hou, H.; Chen, W.; Wang, M. Phase-field simulation for the evolution of solid/liquid interface front in directional solidification process. *J. Mater. Sci. Technol.* **2019**, *35*, 1044–1052. [CrossRef]
22. Sun, Y.; Zhao, Y.; Guo, H.; Tian, X.; Hou, H. Early Stages of Precipitation in γ′ Phase of a Ni-Al-Ti Model Alloy: Phase-Field and First-Principles Study. *Sci. Adv. Mater.* **2020**, *12*, 746–754. [CrossRef]
23. Tian, J.; Zhao, Y.; Hou, H.; Han, P. First-principles investigation of the structural, mechanical and thermodynamic properties of Al_2Cu phase under various pressure and temperature conditions. *Solid State Commun.* **2017**, *268*, 44–50. [CrossRef]
24. Wang, S.; Zhao, Y.; Deng, S.; Yang, W.; Lian, D.; Hou, H. First-principle studies on the mechanical, thermodynamic and electronic properties of β″-Mg_3Gd and β′-Mg_7Gd alloys under pressure. *J. Phys. Chem. Solids* **2019**, *125*, 115–122. [CrossRef]
25. Fan, W.; Chen, R.; Wang, L.; Han, P.; Meng, Q. First-Principles and Experimental Studies of Y-Doped Mg_2Si Prepared Using Field-Activated Pressure-Assisted Synthesis. *J. Electron. Mater.* **2011**, *40*, 1209–1214. [CrossRef]
26. Meng, Q.; Fan, W.; Chen, R.; Munir, Z. Thermoelectric properties of Sc- and Y-doped Mg_2Si prepared by field-activated and pressure-assisted reactive sintering. *J. Alloy. Compd.* **2011**, *509*, 7922–7926. [CrossRef]
27. Stewart, J.C.; Matthew, D.S.; Chris, J.P.; Hasnip, P.J.; Probert, M.J.; Refson, K.; Payne, M.C. First Principles Methods Using Castep. *Z. Kristallogr.* **2005**, *220*, 567–570. [CrossRef]
28. Zhao, Y.; Deng, S.; Liu, H.; Zhang, J.; Guo, Z.; Hou, H. First-principle investigation of pressure and temperature influence on structural, mechanical and thermodynamic properties of Ti_3AC_2 (A = Al and Si). *Comput. Mater. Sci.* **2018**, *154*, 365–370. [CrossRef]
29. Hohenberg, P.; Kohn, W. Inhomogeneous Electron Gas. *Phys. Rev.* **1964**, *136*, B864. [CrossRef]

30. Kohn, W.; Sham, L.J. Self-Consistent Equations Including Exchange and Correlation Effects. *Phys. Rev.* **1965**, *140*, A1133–A1138. [CrossRef]
31. Perdew, J.P.; Burke, K.; Ernzerhof, M. Generalized Gradient Approximation Made Simple. *Phys. Rev. Lett.* **1996**, *77*, 3865. [CrossRef]
32. Hendrik, J.M.; James, D.P. Special points for Brillouin-zone integrations. *Phys. Rev. B* **1976**, *13*, 5188–5192. [CrossRef]
33. Fischer, T.H.; Almlof, J. General methods for geometry and wave function optimization. *J. Phys. Chem.* **1992**, *96*, 9768–9774. [CrossRef]
34. Murtaza, G.; Sajid, A.; Rizwan, M.; Takagiwa, Y.; Khachai, H.; Jibran, M.; Khenata, R.; Bin-Omran, S. First principles study of Mg2X (X = Si, Ge, Sn, Pb): Elastic, optoelectronic and thermoelectric properties. *Mater. Sci. Semicond. Process.* **2015**, *40*, 429–435. [CrossRef]
35. Tani, J.-I.; Kido, H. Lattice dynamics of Mg_2Si and Mg_2Ge compounds from first-principles calculations. *Comput. Mater. Sci.* **2008**, *42*, 531–536. [CrossRef]
36. Grosch, G.; Range, K. Studies on AB2-type Intermetallic Compounds, I. Mg_2Ge and Mg_2Sn: Single-crystal Structure Refinement and Abinitio Calculations. *J. Alloy. Compd.* **1996**, *235*, 250–255. [CrossRef]
37. Liu, Y.; Hu, W.-C.; Li, D.; Zeng, X.-Q.; Xu, C.-S. Predictions of the structural, electronic and thermodynamic properties of the anti-fluorite-type Mg_2Sn under pressure from first principles. *Phys. Scr.* **2013**, *88*, 045–302. [CrossRef]
38. Benhelal, O.; Chahed, A.; Laksari, S. First-principles calculations of the structural, electronic and optical properties of IIA-IV antifluorite compounds. *Phys. Status Solidi B* **2005**, *242*, 2022–2032. [CrossRef]
39. Duan, L.J.; Liu, Y.C. Relationships Between Elastic Constants and EAM/FS Potential Functions for Cubic Crystals. *Acta Metall. Sin.* **2020**, *56*, 112–118. [CrossRef]
40. Nye, J.F. *Physical Properties of Crystals: Their Representation by Tensors and Matrices*; Oxford University Press: New York, NY, USA, 1985.
41. Zhang, X.-D.; Jiang, W. Lattice stabilities, mechanical and thermodynamic properties of Al_3Tm and Al_3Lu intermetallics under high pressure from first-principles calculations. *Chin. Phys. B* **2016**, *25*, 338–347. [CrossRef]
42. Tian, J.; Zhao, Y.; Wang, B.; Hou, H.; Zhang, Y. The structural, mechanical and thermodynamic properties of Ti-B compounds under the influence of temperature and pressure: First-principles study. *Mater. Chem. Phys.* **2018**, *209*, 200–207. [CrossRef]
43. Aydin, S.; Şimşek, M. First-principles calculations of elemental crystalline boron phases under high pressure: Orthorhombic B28 and tetragonal B48. *J. Alloy. Compd.* **2011**, *509*, 5219–5229. [CrossRef]
44. Madelung, O.; Landbolt, B. *Numerical Data and Functional Relationships in Science and Technology*; Springer: Berlin, Germany, 1983.
45. Na-Na, L.; Ren-Bo, S.; Han-Ying, S.; Da-Wei, D. The electronic structure and thermodynamic properties of Mg_2Sn from first-principles calculations. *Acta Phys. Sin.* **2008**, *57*, 7145–7150. [CrossRef]
46. Tani, J.-I.; Takahashi, M.; Kido, H. First-principles calculation of impurity doping into Mg_2Ge. *J. Alloy. Compd.* **2009**, *485*, 764–768. [CrossRef]
47. Davis, L.; Whitten, W.; Danielson, G. Elastic constants and calculated lattice vibration frequencies of Mg_2Sn. *J. Phys. Chem. Solids* **1967**, *28*, 439–447. [CrossRef]
48. Boulet, P.; Verstraete, M.; Crocombette, J.-P.; Briki, M.; Record, M.-C. Electronic properties of the Mg_2Si thermoelectric material investigated by linear-response density-functional theory. *Comput. Mater. Sci.* **2011**, *50*, 847–851. [CrossRef]
49. Zhao, Y.; Wang, S.; Zhang, B.; Yuan, Y.; Guo, Q.; Hou, H. The anisotropy of three-component medium entropy alloys in AlCoCrFeNi system: First-principle studies. *J. Solid State Chem.* **2019**, *276*, 232–237. [CrossRef]
50. Liu, Q.-J.; Liu, Z.-T.; Feng, L.-P.; Tian, H.; Liu, L.; Liu, W.-T. Mechanical and thermodynamic properties of seven phases of $SrHfO_3$: First-principles calculations. *Comput. Mater. Sci.* **2010**, *48*, 677–679. [CrossRef]
51. Tian, J.; Zhao, Y.; Wen, Z.; Hou, H.; Han, P. Physical properties and Debye temperature of Al_7Cu_2Fe alloy under various pressures analyzed by first-principles. *Solid State Commun.* **2017**, *257*, 6–10. [CrossRef]
52. Li, C.; Hoe, J.L.; Wu, P. Empirical correlation between melting temperature and cohesive energy of binary Laves phases. *J. Phys. Chem. Solids* **2003**, *64*, 201–212. [CrossRef]
53. Fu, C.; Wang, X.; Ye, Y.; Ho, K. Phase stability, bonding mechanism, and elastic constants of Mo_5Si_3 by first-principles calculation. *Intermetallics* **1999**, *7*, 179–184. [CrossRef]
54. Otero-De-La-Roza, A.; Abbasi-Pérez, D.; Luaña, V. $Gibbs_2$: A new version of the quasiharmonic model code. II. Models for solid-state thermodynamics, features and implementation. *Comput. Phys. Commun.* **2011**, *182*, 2232–2248. [CrossRef]
55. Wen, Z.; Zhao, Y.; Hou, H.; Wang, B.; Han, P. The mechanical and thermodynamic properties of Heusler compounds Ni_2XAl (X = Sc, Ti, V) under pressure and temperature: A first-principles study. *Mater. Des.* **2017**, *114*, 398–403. [CrossRef]
56. Huang, Z.; Zhao, Y.; Hou, H.; Han, P. Electronic structural, elastic properties and thermodynamics of $Mg_{17}Al_{12}$, Mg_2Si and Al_2Y phases from first-principles calculations. *Phys. B Condens. Matter* **2012**, *407*, 1075–1081. [CrossRef]
57. Ji, D.; Chong, X.; Ge, Z.-H.; Feng, J. First-principles study of pressure-induced phase transformations in thermoelectric Mg_2Si. *J. Alloy. Compd.* **2019**, *773*, 988–996. [CrossRef]
58. Wang, W.; Ren, Y.; Li, Y. First Principles Study of Structural Stability, Elastic Properties, and Electronic Structures of Y-Doped Mg_2Si. *J. Electron. Mater.* **2018**, *48*, 1582–1589. [CrossRef]